Accepted Manuscript

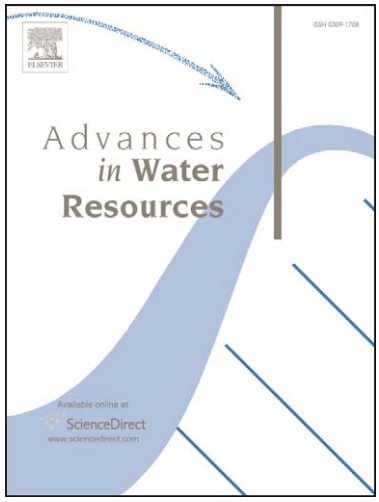

Tidal influence on BTEX biodegradation in sandy coastal aquifers

C. Robinson, A. Brovelli, D.A. Barry, L. Li

PII: S0309-1708(08)00164-4
DOI: 10.1016/j.advwatres.2008.09.008
Reference: ADWR 1332

To appear in: *Advances in Water Resources*

Received Date: 3 April 2008
Revised Date: 14 September 2008
Accepted Date: 18 September 2008

Please cite this article as: Robinson, C., Brovelli, A., Barry, D.A., Li, L., Tidal influence on BTEX biodegradation in sandy coastal aquifers, *Advances in Water Resources* (2008), doi: 10.1016/j.advwatres.2008.09.008

This is a PDF file of an unedited manuscript that has been accepted for publication. As a service to our customers we are providing this early version of the manuscript. The manuscript will undergo copyediting, typesetting, and review of the resulting proof before it is published in its final form. Please note that during the production process errors may be discovered which could affect the content, and all legal disclaimers that apply to the journal pertain.

ACCEPTED MANUSCRIPT

Tidal influence on BTEX biodegradation in sandy coastal aquifers

C. Robinson[1,#], A. Brovelli[1], D.A. Barry[1] and L. Li[2,3]

[1]*Laboratoire de technologie écologique, Institut des sciences et technologies de l'environnement, Station No. 2, Ecole Polytechnique Fédérale de Lausanne, CH-1015 Lausanne, Switzerland. E-mails: clare.robinson@epfl.ch, alessandro.brovelli@epfl.ch, andrew.barry@epfl.ch*

[2]*Environmental Engineering Division, School of Engineering, The University of Queensland, St. Lucia QLD 4072, Australia. E-mail: l.li@uq.edu.au*

[3]*Centre for Eco-Environmental Modelling, Hohai University, Nanjing 210098, P. R. China. E-mail: Li_LingCJ@hhu.edu.cn*

Revised version submitted to *Advances in Water Resources* on 14 September 2008

[#] Author to whom correspondence should be addressed. Tel.: +41 21 693 2757; Fax: +41 21 693 5670

ACCEPTED MANUSCRIPT

Abstract

A numerical study was conducted to investigate the influence of tides on the fate of terrestrially-derived BTEX discharging through an unconfined aquifer to coastal waters. Previous studies have revealed that tide-induced seawater circulations create an active salt-freshwater mixing zone in the near-shore aquifer and alter the specific subsurface pathway for contaminants discharging to the coastal environment. Here the coupled density-dependent flow and multi-species reactive transport code PHWAT was used to examine the impact of these tidal effects on the aerobic biodegradation of BTEX released in a coastal aquifer and its subsequent loading to coastal waters. Simulations indicated that tides significantly enhance BTEX attenuation in the near-shore aquifer. They also reduce the rate of chemical transfer from the aquifer to the ocean and exit concentrations at the beach face. For the base case consisting of toluene transport and biodegradation, 79% of toluene initially released in the aquifer was attenuated prior to discharge with tides present, compared to only 1.8% for the non-tidal case. The magnitude of tidal forcing relative to the fresh groundwater flow rate was shown to influence significantly the extent of biodegradation as it controls the intensity of salt-freshwater mixing, period of exposure of the contaminant to the mixing zone and rate of oxygen delivery to the aquifer. The oxygen available for biodegradation also depends on the rate at which oxygen is consumed by natural processes such as organic matter decomposition. While simulations conducted with heterogeneous conductivity fields highlighted the uncertainties associated with predicting contaminant loadings, the study revealed overall that BTEX may undergo significant attenuation in tidally-influenced aquifers prior to discharge.

Keywords: Aquifer-ocean exchange; Subterranean estuary; Submarine groundwater discharge; Coastal water pollution.

ACCEPTED MANUSCRIPT

1. Introduction

Contamination of coastal aquifers is a growing problem due to increasing populations and developments in coastal areas. There is a need for effective assessment of the fate of contaminants released in such environments as their transport to coastal waters via submarine groundwater discharge (SGD) can lead to significant degradation of receiving coastal ecosystems [1-4]. In addition these contaminants can disturb the habitat condition in the interstitial beach environment for a wide range of flora and fauna [5]. The combined influences of oceanic oscillations, terrestrial groundwater discharge and variable-density effects result in complex and dynamic flow, transport and biogeochemistry in a near-shore aquifer [6-9]. These processes alter contaminants' subsurface transport pathway and subsequent fate. Therefore they need to be quantified to estimate contaminant loading to coastal waters. As a large proportion of the world's coastlines are exposed to significant tidal fluctuations, this study examines the effect of tides on the fate of subsurface reactive contaminants, in particular BTEX, released in a coastal aquifer.

The groundwater flow and salt transport processes in a tidally-influenced aquifer have previously been investigated via numerical modeling [10-14], field measurements [7,15-17] and laboratory experiments [18,19]. It has been revealed that the salinity structure in a tidally-influenced aquifer is characterized by two distinct saline plumes: the classical saltwater wedge and an upper saline plume [16,17,19,20]. These two plumes confine a freshwater discharge zone in which fresh groundwater discharges near the low tide mark rather than around the shoreline as occurs in the absence of tidal forcing [16,19]. While the saltwater wedge develops due to the density contrast between seawater and fresh groundwater [21,22], the upper saline plume is

ACCEPTED MANUSCRIPT

formed primarily by tides. Tidal action drives seawater recirculation through the near-shore aquifer at significant rates compared with fresh groundwater discharge [23,24]. The asymmetric flow associated with tidal forcing across a sloping beach results in a tide-averaged circulation cell, whereby water infiltrates the beach in the upper inter-tidal zone and exfiltrates near the low tide mark (Figure 1a) [11,12,16,18]. Advective salt transport associated with this circulation is responsible for the development of the upper saline plume [16].

Due to their distinct chemical compositions, the mixing of the recirculating seawater and discharging fresh groundwater sets up a potentially important biogeochemical reaction zone in the near-shore aquifer. This mixing zone, called a subterranean estuary [25], has significant implications for the fate of subsurface reactive contaminants discharging to coastal waters [8,26]. While the dispersion zone of the salt-water wedge has traditionally been viewed as the primary area of mixing between fresh groundwater and recirculating seawater in a subterranean estuary [25], it has recently been shown that the upper saline plume is perhaps a more active and dynamic zone of mixing as it is associated with faster flow rates and shorter residence times [10]. Furthermore dissolved oxygen and pH measurements have revealed potentially important redox and pH zonations associated with this upper plume [7].

Recently Robinson et al. [10] presented numerical tracer simulations to illustrate tidal influence on the subsurface transport pathway of conservative land-derived contaminants discharging to coastal waters. The simulations indicated that tides may reduce the impact of a contaminant by modifying significantly its specific discharge pathway and the geochemical conditions along this pathway. In particular it was shown that tides may decrease the rate of chemical transfer from the aquifer to the

ACCEPTED MANUSCRIPT

ocean and lower the exit concentrations of chemicals at the interface. With tides present the tracer migrated through the upper saline plume. While it was hypothesized that the geochemical conditions in this mixing zone would likely affect the fate of a reactive contaminant and its subsequent flux to coastal waters, reactive processes were not simulated.

Groundwater contamination by BTEX (benzene, toluene, ethylbenzene and xylenes) due to the unintentional release of petroleum hydrocarbons is a widespread problem. With many airports, refineries and bulk terminals located in coastal areas, these compounds are commonly found in coastal aquifers and can find their way to marine and estuarine environments via submarine groundwater discharge. As discussed above the tidal effects in the near-shore aquifer could influence the attenuation of these contaminants prior to their release to coastal waters. The transport and biodegradation of toluene in a tidally-influenced aquifer has been simulated by Li et al. [27]. While they demonstrated that tides lead to the creation of an oxygen-rich zone near the shoreline resulting in enhanced biodegradation of toluene, simulations were performed using a constant density groundwater flow model. As density variations strongly influence the flow patterns, mixing conditions and thus biogeochemical zonations in a near-shore aquifer, there remains a need to examine the reactive processes with consideration of the variable density effects. A series of laboratory and numerical experiments have been performed to examine the bioremediation of tidally-influenced beaches that have been contaminated by offshore oil spills [19,28,29]. These experiments concentrated on understanding the effect of tides on flow and transport dynamics in the beach groundwater system to enable effective design of nutrient treatment strategies required to remediate the oil-polluted beach zone (typically the top 25 cm of

ACCEPTED MANUSCRIPT

sand in the intertidal zone). While variable-density effects were considered, reactive processes were not simulated in the studies.

Field data on the biodegradation of BTEX in coastal aquifers, in particular tidally-influenced systems, is sparse. Westbrook et al. [30] presented a field investigation of a dissolved BTEX groundwater plume flowing towards a tidally and seasonally forced estuarine river. They demonstrated that tidal fluctuations lead to the formation of a hyporheic zone that strongly influenced the distribution of BTEX compounds near the shore and their spatial and temporal discharge patterns. Although a follow-up modeling study was conducted by Trefry et al. [31], the focus of this modeling was the influence of density and seasonal variations on the subsurface flow and transport mechanisms rather than the tidal effects and reactive processes. Collection of field data to assess the extent of BTEX attenuation in a near-shore aquifer prior to discharge is a challenging task. Direct measurement of the compounds in the aquifer is difficult given the complex and dynamic nature of tidally-influenced groundwater systems. Furthermore, biodegradation rates likely increase markedly in the vicinity of the aquifer-ocean interface as interaction between the contaminated plume and recirculating seawater intensifies. Indirect measurement via detection of the BTEX in the coastal water is also near impossible because dilution occurs immediately as it is discharged. Despite the simplifications involved, reactive contaminant transport modeling is able to provide an evaluation of the extent of biodegradation in the subsurface and thus the risks associated with BTEX groundwater contamination and its impact on the receiving coastal ecosystem.

Here we investigate the fate of BTEX released in a tidally-influenced unconfined coastal aquifer using the coupled density-dependent groundwater flow and multi-

ACCEPTED MANUSCRIPT

species reactive transport code PHWAT [32], with the overall aim of quantifying the tidal effects on biodegradation. The reactive processes are simulated using an aerobic biodegradation model. The competitive consumption of oxygen by alternative electron donors such as naturally-occurring organic matter is also considered as these processes influence the subsurface oxygen availability. Simulations with and without tides are presented to illustrate the tidal effects on the extent of attenuation and thus contaminant flux across the aquifer-ocean interface. Following this, the impact of natural oxygen consumption rates and the relative magnitude of inland (fresh groundwater flow rate) and tidal (tidal amplitude) forcing on the fate of BTEX are examined. Finally simulations performed using heterogeneous hydraulic conductivity fields are discussed to demonstrate the uncertainties associated with predictions of contaminant fluxes to coastal waters.

2. Numerical Simulations

The transport and biodegradation of a dissolved BTEX plume in an unconfined near-shore aquifer subject to tidal forcing was simulated using PHWAT [32]. This program couples the density-dependent groundwater flow and solute transport model, SEAWAT [33], with the geochemical reaction model, PHREEQC-2 [34].

2.1 Groundwater flow and solute transport model

The numerical model used to simulate the variable-density groundwater flow and solute transport processes in a tidally-influenced aquifer is a modified version of that presented and described by Robinson et al. [10]. The model description is recapped briefly here. Tidal forcing across a sloping beach face is simulated using a two zone approach with surface water (zone A) and aquifer (zone B) zones. A schematic

ACCEPTED MANUSCRIPT

of the model domain, including the boundary conditions and parameter values used, is provided in Figure 2. The model represents a cross-shore transect through a coastal aquifer where the *x*-*z* co-ordinate origin is located at the mean shoreline. The model domain extends 100 m landward and 40 m seaward of the mean shoreline. The aquifer depth (*H)* is 10 m representing a shallow coastal groundwater system. The beach slope (tanβ), as represented by the boundary between zones A and B, is 0.1.

High hydraulic conductivity (10^6 m d^{-1}), porosity (n_e) = 1 and constant salt concentration of 35 g l^{-1} are assigned to cells in zone A to represent the coastal surface water. Tidal forcing is simulated by applying a time-varying head (h_{tide}) to selected cells in zone A (Figure 2):

$$h_{tide} = A\cos\omega t + H\,, \tag{1}$$

where A (m) is the tidal amplitude, t (d) is time and ω (Rad d^{-1}) is the tidal angular frequency. For the base simulations A = 0.75 m and ω = 12.567 Rad d^{-1} (semi-diurnal tidal period = 0.5 d). The high hydraulic conductivity assigned to surface water cells allows for nearly instantaneous transmission of h_{tide} to the submerged beach face. The aquifer (zone B) is isotropic and homogeneous with hydraulic conductivity (K) = 15 m d^{-1}, n_e = 0.25, longitudinal dispersivity (α_L) = 0.2 m and transverse dispersivity (α_T) = 0.02 m.

The interface between the ocean and aquifer is a complex boundary for model simulations. With SEAWAT-2000 it is not possible to simulate the formation of a seepage face on this boundary on the ebbing tide. The model also neglects variably saturated flow. These limitations have been discussed in detail by Robinson et al. [10]. While seepage face dynamics could affect predicted discharge rates across the interface and consequently the BTEX exit concentrations, the boundary conditions

ACCEPTED MANUSCRIPT

and aquifer parameters used were specifically chosen to represent conditions under which seepage face formation is limited (i.e., beach slope = 0.1).

A uniform, constant flux (Q_f = 0.5 m^2 d^{-1}) is specified along the landward vertical boundary to simulate the terrestrial groundwater flow. No flow is specified along the bottom and seaward vertical boundaries. The upper boundary is a phreatic surface with negligible groundwater recharge.

Numerical tests were performed to ensure that model solutions are independent of the grid discretization. The model presented has 56 columns and 49 layers. The grid is non-uniform with refinement around the aquifer-ocean interface. As tidal phase-resolving simulations are computationally intensive, models are initially run to the steady state with no tide. Tidal fluctuations are then introduced and the models are run to the quasi-steady state with respect to both heads and salt concentrations. Once this solution is reached the contaminant is released as a pulse to the aquifer through a point source and the model is run until a negligible amount of contaminant remains in the aquifer. Using an Intel Xeon 3.2GHz running Ubunta Linux (kernel version 6.22), the model runs took approximately 5 d to reach quasi-steady state for the conservative transport simulations and approximately 15 d to reach quasi-steady state when the geochemical reaction model was included.

2.2 BTEX injection and geochemical reaction model

Following the numerical tracer simulations presented in Robinson et al. [10], the contaminant is injected into an initially uncontaminated aquifer through a point source located 30 m landward of the shoreline at the watertable (Figure 2). Also following Robinson et al. [10] the contaminant release occurs as a pulse over 1 d with a

ACCEPTED MANUSCRIPT

flow rate of 0.1 m^3 d^{-1}. The concentrations of species in the contaminant source are provided in Table 1. Only toluene was injected for the base simulations; however further simulations were performed with all BTEX compounds (toluene, benzene, ethylbenzene, xylenes) present. Simulation of a pulse injection provides a clear illustration of the influence of tides on the transport and biodegradation of BTEX as it discharges through a near-shore aquifer. In many cases, however, BTEX spills can lead to a NAPL source on the water table that produces a continuous input of contaminants to the aquifer. Therefore the implications of the pulse injection results for a continuous source are also discussed.

The biodegradation of BTEX is typically controlled by the availability of suitable electron acceptors (e.g., oxygen, sulfate, nitrate) [35]. Here, oxygen is considered to be the sole electron acceptor. The rate of attenuation of each BTEX compound (R_i, mol d^{-1}) is described using Monod biodegradation kinetics [35]:

$$R_i = -\frac{\mu_{max\_i} C_i}{K_{s\_i} + C_i} \frac{C_O}{K_{s\_O} + C_O} X_b, \quad (2)$$

where C_i (mol l^{-1}) is the concentration of BTEX compound i (toluene, benzene, ethylbenzene or xylenes), C_O (mol l^{-1}) is the oxygen concentration, μ_{max_i} (d^{-1}) is the specific maximum biodegradation rate of compound i, K_{s_i} (mol l^{-1}) is the half saturation constant for the biodegradation of each compound and K_{s_O} (mol l^{-1}) is the half saturation constant for the effect of oxygen on the biodegradation of BTEX. X_b (mol l^{-1}) is the biomass concentration of aerobes with an overall population growth rate given by:

$$\frac{dX_b}{dt} = \sum_{i=1,n} R_i Y_i - b_b X_b, \quad (3)$$

ACCEPTED MANUSCRIPT

where Y_i is the biomass yield coefficient related to the consumption of BTEX compound i, b_b (d^{-1}) is the aerobe decay coefficient and n is the number of BTEX compounds involved. The model assumes that the biomass is immobile and the effects of bioclogging on the flow processes are negligible. For the initial simulations only toluene is considered, thus n = 1. The aerobic biodegradation reactions and Monod parameter values adopted for each BTEX compound are provided in Table 2.

The consumption of oxygen as BTEX degrades is calculated based on the reaction stoichiometry provided in Table 2. In intertidal sediments natural processes such as organic matter decomposition and oxidation of reduced inorganic species (e.g., H_2S, Fe^{2+}, Mn^{2+}) also consume oxygen [36], thus reducing its availability for BTEX biodegradation. We adopt a first-order rate expression to describe the natural oxygen-consuming processes. The total oxygen consumption is simulated by:

$$\frac{dC_O}{dt} = -\sum_{i=1,n_{org}} R_i S_i - b_O C_O, \quad (4)$$

where S_i is the oxygen stoichiometric coefficient for the biodegradation of BTEX compound i (Table 2) and b_O (d^{-1}) is the first-order rate constant for natural oxygen consumption. A general first-order rate expression is used rather than individually simulating the natural oxygen-consuming processes due to the significant reduction in computational effort. The model assumes that different microbial populations are responsible for the natural oxygen-consuming processes and BTEX biodegradation. As such the natural oxygen consumption rate does not influence the concentration of aerobes. While first-order kinetics have previously been used to describe oxygen consumption in sediments [e.g., 37], we were unable to find a literature value for b_O applicable to the intertidal beach environment. A realistic value for b_O (= 0.09 d^{-1}) was determined by performing sensitivity analyses and comparing simulated oxygen dis-

ACCEPTED MANUSCRIPT

tributions with measurements collected in intertidal sediments subject to similar forcing conditions [7] (Section 3.1). The influence of b_O on the extent of toluene attenuation was also investigated and the results are discussed in Section 3.5.

The concentrations of oxygen, biomass and salt in the contaminant source, initial concentrations in Zone B, concentrations in the terrestrial fresh groundwater (Q_f) and constant concentrations in Zone A are provided in Table 1. Most notably the fresh discharging groundwater and contaminant source are anaerobic with dissolved oxygen concentrations of 0.025 mmol l^{-1}, whereas the seawater is aerobic with near-saturated dissolved oxygen concentrations (0.25 mmol l^{-1}) [37].

3. Results and Discussion

3.1 Tide-induced salinity and oxygen distributions

Simulated salinity and oxygen distributions in a tidally-influenced aquifer are shown in Figure 1. The upper saline plume formed by tide-induced seawater circulations through the intertidal zone is present in addition to the classical saltwater wedge (Figure 1a). As the recirculating seawater transports both salt and oxygen from the ocean into the aquifer, the predicted salt and oxygen distributions are identical, but with different magnitudes, when natural oxygen consumption is not simulated (i.e., b_O = 0 d^{-1}; Figures 1a and b). Field data collected in a sandy intertidal aquifer indicate however that the salt and oxygen distributions vary significantly [7]. While Robinson et al. [7] observed two distinct saltwater plumes (upper saline plume and saltwater wedge), high oxygen content was present only in the upper intertidal region. The measurements indicated that the recirculating seawater maintained relatively high oxygen content close to the infiltration zone in the upper intertidal region but oxygen was rapidly consumed along its flow path. Oxygen consumption was most significant

ACCEPTED MANUSCRIPT

in the subtidal zone where low oxygen concentrations were measured despite high local salinities. The absence of oxygen in this zone is attributed to not only the longer residence times associated with density-driven recirculating seawater but also to a typically higher abundance of organic matter and microbial activity in subtidal, as compared to intertidal, sediments [38-40]. Other studies have also reported oxygenated sediments up to 4 m below the beach surface in intertidal sediments, as opposed to a few centimeters of oxygen penetration in subtidal sediments [39,41].

Figure 1c shows the simulated oxygen distribution with b_O = 0.09 d^{-1}. In adopting this first-order rate constant to simulate the natural oxygen-consuming processes, the model predicts a similar subsurface oxygen distribution to the field observations of Robinson et al. [7]. Note that such an oxygen distribution indicates that oxygen is available for BTEX biodegradation, as in the following simulations. However, in contrast to the field data reported in [7] a zone of elevated oxygen content is predicted in the subtidal region in addition to the zone in the upper intertidal region. This discrepancy arises because b_O is constant, implying that concentrations and reactivity of organic matter, reduced inorganic species and microorganisms are uniform in the near-shore aquifer.

3.2 Transport and biodegradation of toluene

The transport of toluene through a near-shore aquifer with aerobic biodegradation considered is shown in Figures 3 and 4 for non-tidal and tidal conditions, respectively (b_O = 0.09 d^{-1} in these simulations). In the absence of tidal fluctuations toluene moves seaward along the top of the aquifer and discharges close to the shoreline (Figures 3a-c). While the contaminant plume disperses as it moves seaward, it does not mix significantly with the oxygenated recirculating seawater (Figures 3g-i). Conse-

ACCEPTED MANUSCRIPT

quently, the biodegradation of toluene prior to discharge is negligible, as indicated by the low growth of biomass near the shoreline (Figures 3d-f). This is further evident in Figure 5a where the mass of toluene remaining in the aquifer following injection is nearly identical to the simulation without biodegradation. The limited biomass growth and oxygen consumption as toluene is transported through the near-shore aquifer can be seen in Figures 5b and c, respectively.

Figure 4 shows that tidal fluctuations modify significantly the specific discharge pathway for toluene. Toluene first migrates seaward along the top of the aquifer but as it approaches the intertidal region it is transported downwards by the tide-induced flow circulations (Figures 4a-c). Here toluene mixes with the oxygenated recirculating seawater (Figures 4g-i) and aerobic biodegradation occurs along with biomass growth (Figures 4d-f). Biodegradation and thus biomass growth are most significant in the upper intertidal zone due to the higher oxygen and also toluene concentrations there. The biomass growth and simultaneous oxygen consumption that occurs as toluene degrades in the intertidal zone is evident in Figures 5b and c. The total biomass in the aquifer reaches a maximum around 122.5 d. Following this time the biomass decay rate exceeds its growth rate from biodegradation, and the total biomass population decreases until the initial unperturbed conditions are reached. The total subsurface oxygen content is lowest around 127 d. After this time the delivery rate of oxygen to the subsurface by the recirculating seawater exceeds the rate at which oxygen is consumed by both toluene biodegradation and the competing natural processes. Oxygen concentrations continue to increase until the oxygen input rates and consumption rates reach the initial quasi-equilibrium conditions.

ACCEPTED MANUSCRIPT

To quantify the extent of biodegradation occurring in the subsurface prior to discharge, the total mass (moles) of BTEX compound *i* discharging across the aquifer-ocean interface (I_{d_i}) was calculated by:

$$I_{d\_i} = \int_0^{t_{final}} \int_{surf} qC_i \, ds \, dt, \tag{5}$$

where q is the specific discharge across the interface ($m^2\ d^{-1}$) and s is the distance along the interface (m). A percentage removal efficiency was then determined using,

$$\text{Removal Efficiency} = \frac{I_{0\_i} - I_{d\_i}}{I_{0\_i}} \times 100, \tag{6}$$

where I_{0_i} is the initial moles of BTEX compound *i* released into the aquifer. The simulations predict that with tides present the removal efficiency for toluene is 79% compared with 1.8% for non-tidal conditions. This reveals that for the simulated conditions tidal forcing strongly influences the transformation of toluene in the subsurface and thus its impact on the interstitial beach environment and near-shore coastal waters.

In addition to enhancing the attenuation of toluene in the near-shore aquifer, tidal forcing also increases the subsurface residence time of the contaminant (Figure 5a). Based on the mass remaining in the aquifer following injection (without biodegradation), the mean residence time of toluene in the subsurface increases from 90.5 to 140 d when tides are included. This increase is due primarily to the lengthening of toluene's transport path [10]. With biodegradation included, toluene's mean subsurface residence time is reduced to 126 d for the tidal case as opposed to only 90 d for the non-tidal case; thus further illustrating the limited attenuation of toluene in the absence of tides. The total chemical flux across the aquifer-ocean interface behaves si-

ACCEPTED MANUSCRIPT

milarly for tidal and non-tidal conditions, but with a time lag of approximately 50 d for the tidal conditions (Figure 6). The maximum toluene flux across the interface occurs at 82 d and 140 d for the non-tidal and tidal simulations respectively. For the non-tidal conditions, the difference between toluene's mean residence time (90 d) and time at which the toluene flux across the interface is the greatest (82 d) indicates that for these conditions the mass discharge pattern is slightly asymmetrical. In Figure 6 it can be seen that tides also increase the longitudinal spread of toluene as indicated by the chemical flux across the interface occurring over a longer period of time. This longitudinal spread significantly reduces the maximum flux as shown by the tidal simulation without biodegradation (−×− in Figure 6). As expected, the chemical flux is further lowered when biodegradation is considered (− − in Figure 6).

Perhaps more significantly, the toluene exit concentrations at the beach face are over an order of magnitude lower with tides present and are again reduced when biodegradation is considered (Figure 7). This suggests that the threat of groundwater-borne contaminants on the interstitial beach and near-shore ecosystems is likely markedly reduced by tidal effects. For conservative contaminants (i.e., without biodegradation, Figures 7a and c), such reduction in exit concentrations is due primarily to the mixing and dilution of the contaminant with the tidally-driven recirculating seawater. As indicated by the wider discharge zone for tidal conditions (Figure 7c), tides also enhance the transverse spread of toluene. Here toluene discharges largely around the low tide mark (x = 47.5 m) as opposed to the vicinity of the shoreline for the non-tidal case. Thus, in summary, these simulations indicate that for certain conditions, tidal effects could significantly enhance the natural attenuation of toluene in the near-shore aquifer prior to discharge and thereby reduce the need for engineered remediation schemes. It is important to note that in these simulations oxygen is the sole electron

ACCEPTED MANUSCRIPT

acceptor for biodegradation and if other acceptors were also considered (e.g., sulfate, nitrate) then biodegradation rates would likely increase further.

In many cases, spills of BTEX produce a continuous input of BTEX to the aquifer over a longer period than simulated here by a relatively short pulse injection. For a continuous source, the extent of toluene biodegradation would over time reach a steady value whereby the amount of biodegradation occurring would match the rate at which oxygen is delivered to the mixing zone by the tidal circulations, minus that consumed by the competing natural processes (taking into account the biodegradation stoichiometry, Table 2). For the conditions simulated, as it was shown that the rate of oxygen consumption by both toluene biodegradation and the natural processes was greater than the rate of oxygen input to the subsurface (Figure 5c), it is expected that, for a continuous input with a similar source concentration and flow rate, the extent of biodegradation will reduce over time until the system reaches steady state. At this time the rate of biodegradation will correspond to the rate of oxygen delivery to the intertidal subsurface mixing zone.

3.3 Biodegradation of other BTEX compounds

The transport and biodegradation of a contaminant plume containing toluene as well as benzene, ethylbenzene and xylenes was also simulated to evaluate the influence of tides on the attenuation of these additional BTEX compounds. The aquifer parameters, forcing conditions and contaminant release were the same as for the simulations presented above but the composition of the injected contaminant solution was varied (Table 1). The ratio of the BTEX compounds in the solution was based on Barry et al. [35].

ACCEPTED MANUSCRIPT

Toluene is predicted to have the highest removal efficiency (46%), followed by benzene (37%), ethylbenzene (36%) and finally xylenes (33%). Due to increased competition and thus reduced oxygen availability in the intertidal aquifer, the extent of toluene attenuation decreases from 79% to 46% when the other BTEX species are present. For non-tidal conditions the extent of biodegradation in the near-shore aquifer is again limited with removal efficiencies less than 2% for all the compounds considered.

The chemical fluxes across the aquifer-ocean interface for each compound with and without tidal forcing are shown in Figures 8a and b, respectively. The temporal behavior of the chemical flux is similar for all compounds with the magnitude varying according to the initial mass injected and the extent of biodegradation. Similar to the simulations with only toluene injected, tides are shown to increase the contaminants' subsurface residence time. In addition, as discharge occurs over a longer period the maximum chemical fluxes are reduced. The maximum chemical flux occurs approximately 140 d after injection for tidal conditions compared with 82 d for non-tidal conditions. The exit concentrations at these times are shown in Figures 8c and d, indicating the maximum expected contaminant concentrations at the beach face. For comparison, the WHO guideline values for drinking-water quality [42] for each species are also indicated in Figures 8c and d. The WHO guidelines for safe recreational water environments [43] suggest using these drinking-water quality guideline values as a basis for screening the potential risk of a particular contaminant. If the drinking-water guideline value is exceeded, it is recommended that a specific evaluation of the risk of the contaminant is undertaken. By comparing the exit concentrations with the guideline values [42], it can be seen that while the exit concentrations significantly exceed the guideline values for non-tidal conditions, with tides present the concentrations are

ACCEPTED MANUSCRIPT

reduced to an acceptable level for all components except benzene. Benzene has the highest maximum exit concentration, however as it is the most toxic and carcinogenic compound it also has the lowest guideline value. Even with tides present, for the conditions simulated, the predicted benzene exit concentrations are more than 50 times greater than the guideline concentration. This suggests that remediation technologies may need to be implemented to reduce benzene concentrations to an acceptable level prior to its release to coastal waters even in tidally-influenced environments.

3.4 Magnitude of tidal and inland forcing

Due to enhanced seawater recirculation and thus increased oxygen availability and mixing between the discharging fresh groundwater and recirculating seawater in the near-shore aquifer, the model predicts that toluene attenuation increases significantly as the tidal amplitude increases (Figure 9a). Despite the complexity of the reactive processes, for small tidal amplitude the removal efficiency increases directly with the amplitude. This correlates with a linear increase in the tidally-driven seawater recirculation rates (Q_t, Figure 9b). The relationship becomes non-linear as the removal efficiency approaches 100% (asymptote).

Robinson et al. [10,24] revealed however that it is the balance between the tidal and inland forcing which controls the subsurface flow patterns and mixing conditions in a tidally-influenced aquifer, rather than just the tidal amplitude. This ratio is important because, as the seaward-directed fresh groundwater flow increases, the tidal circulations through the intertidal region become restricted resulting in a reduction in the seawater recirculation rate and mixing intensity. Robinson et al. [10] showed that the extent of mixing in a tidally-influenced aquifer can be determined based on the ratio of the fresh groundwater discharge (Q_f) to the tidally-driven seawater recircula-

ACCEPTED MANUSCRIPT

tion (Q_t). Using this ratio near-shore aquifer systems were classified as either stratified, partially-stratified (partially-mixed) or well-mixed. Here we examined the ensuing affect of this ratio on the subsurface attenuation of toluene by performing simulations with varying tidal amplitude and Q_f. As expected the removal efficiency of toluene increases as this flow ratio decreases, i.e., as the tidal forcing strengthens relative to the inland forcing (Figure 10). It is expected that as this ratio approaches zero and the inland flow becomes negligible relative to the tidal recirculation, the system will become completely mixed and the extent of biodegradation will approach 100% biodegradation. In addition to the flow ratio influencing the mixing conditions and oxygen availability, toluene's subsurface residence time increases as the flow ratio decreases (i.e., Q_f decreases). As a result the time for toluene to interact with the reactive mixing zone increases and thus the attenuation of toluene is enhanced.

3.5 Influence of natural oxygen-consuming processes

The extent of toluene attenuation in the near-shore aquifer is strongly influenced by not only the physical forcing mechanisms, which affect the contaminants' specific flow path and extent of salt-freshwater mixing, but also the availability of oxygen in the mixing zone. This availability is controlled by the rate of oxygen input to the subsurface relative to the rate of oxygen consumption. Whilst the former depends on the physical forcing (i.e., tidal beaches with higher seawater recirculation have greater oxygen input), prediction of the rate of oxygen consumption by natural processes is complicated as it depends on factors such as organic matter loading, concentration of reduced species (e.g., Fe^{2+}, Mn^{2+}, H_2S), mineralogy and microbial activity [36,37,44].

ACCEPTED MANUSCRIPT

By varying the first-order rate constant b_O, the effect of the rate of natural oxygen consumption on the biodegradation of toluene was investigated. For the same physical forcing conditions, the subsurface oxygen content increases as the rate of the natural oxygen consumption decreases (i.e., b_O decreases; Figure 11a). As b_O approaches zero the total mass of oxygen in the near-shore aquifer increases significantly. This is because the density-driven recirculating seawater associated with the saltwater wedge maintains a high oxygen content despite its slow flow rate and long residence time (i.e., Figure 1b). In contrast, as b_O increases the total oxygen content in the aquifer approaches an asymptotic lower limit, the value of which is determined by the specified minimum subsurface oxygen concentration (10^{-5} mol l^{-1}). As expected the attenuation of toluene increases as the oxygen available for biodegradation increases (Figure 11b). Enhanced biodegradation as b_O decreases is also evident in Figure 5a where toluene is removed from the aquifer more rapidly when b_O = 0 d compared with b_O = 0.09 d^{-1}. The oxygen consumed and biomass produced by toluene biodegradation also increases as b_O decreases (Figures 5b and c).

From Figure 11 it can be seen that the significant increase in subsurface oxygen content as b_O approaches zero is only accompanied by a slight increase in toluene's removal efficiency. This is because the increasing oxygen concentrations are not associated with the recirculating seawater which participates in the intertidal mixing process, but rather with the seawater recirculating through the subtidal sediments. For low b_O the amount of biodegradation is limited by the actual extent and time available for mixing prior to the contaminants' discharge, but as b_O increases biodegradation becomes limited instead by the low oxygen availability in the mixing zone. For the conditions simulated, as b_O increases from 0.15 to 0.5 d^{-1} although the total subsurface oxygen content decreases only slightly, toluene's removal efficiency decreases from

ACCEPTED MANUSCRIPT

61% to 14%. This is because for this range of b_O, oxygen becomes depleted particularly in the intertidal fresh-saltwater mixing zone where the majority of biodegradation otherwise occurs.

This sensitivity analysis indicates that the b_O value (0.09 d^{-1}) we have adopted for the base conditions results in a comparatively high removal efficiency of toluene. This value is appropriate for the tidal simulations because high-energy sandy beaches are typically well-drained with low organic matter content and thus relatively high oxygen content [5,38]. However b_O was also set to 0.09 d^{-1} for the non-tidal simulations. Here we have likely over-predicted the subsurface oxygen concentrations and removal of BTEX as lower energy beaches typically have higher concentrations of organic matter and microorganisms and thus higher b_O. However, as simulations predict that the removal efficiency of toluene approaches zero for non-tidal conditions, the influence of using a low b_O is trivial as the extent of biodegradation is limited by the negligible mixing between recirculating seawater and the discharging groundwater rather than the competitive consumption of oxygen.

3.6 Influence of aquifer heterogeneity

The results presented thus far assume an isotropic and homogeneous aquifer. Additional simulations were conducted to illustrate the variations introduced by a heterogeneous flow field and thus uncertainty associated with predicting the attenuation of BTEX in a tidally-influenced aquifer. Heterogeneous hydraulic conductivity fields were produced using the random log-normal field generator available within Processing Modflow for Windows (PMWIN) [45]. The generated fields have a mean K = 15 m d^{-1}, standard deviation (base 10) = 0.5 and correlation length/overall model length = 0.1. The standard deviation and correlation length adopted are based on a summary of

ACCEPTED MANUSCRIPT

field data compiled by Gelhar [46] which shows that, at most sites (including sandy aquifers), the standard deviation is between 0.4 and 1, and for overall scales less than 1 km, the correlation length is around 10% of the overall scale. Simulations were performed using four different heterogeneous conductivity fields (fields 1-4). Except for the hydraulic conductivity, the models were identical to the base tidal simulation (Section 3.2).

While the removal efficiency of toluene is 79% for the homogeneous conditions, this efficiency varies from 68% (field 1) to 91% (field 4) with heterogeneities present. The rates of toluene flux across the aquifer-ocean interface for these simulations are shown in Figure 12. With the correlation scale and standard deviation used, toluene's average subsurface residence time varies significantly for the different cases and the extent of biodegradation changes accordingly. For field 1 toluene is rapidly transported through the aquifer along a preferential flow path with its mean residence time (without biodegradation) decreasing to 94.7 d compared with 140 d for homogeneous conditions. As the time for toluene to interact with the reactive mixing zone is reduced, the biodegradation of toluene decreases (removal efficiency of 68%). In comparison, for fields 2 and 4, toluene's average subsurface residence time (without biodegradation) is increased to 202 and 226 d respectively, resulting in higher removal efficiencies of 88% and 91%. Heterogeneities also modify the seawater recirculation patterns and thus oxygen distribution in the intertidal sediments. This effect is illustrated by the simulation performed with field 3 where although toluene's average residence time is larger (159 d) than for homogeneous conditions, the removal efficiency is reduced (74%). The reduced attenuation is attributed to lower rates of seawater recirculation through the intertidal region and thus less subsurface oxygen available in the mixing zone for biodegradation.

ACCEPTED MANUSCRIPT

Heterogeneities also enhance the longitudinal spread of toluene as it is transported through the aquifer (Figure 12). While the temporal behavior of the chemical flux is relatively symmetrical for homogeneous conditions, heterogeneities lead to a highly unsymmetrical discharge pattern with marked tailing. This is particularly evident for the case of no biodegradation (Figure 12a). The tailing is reduced when biodegradation is considered as toluene is more susceptible to attenuation the longer it remains in the subsurface (Figure 12b). Heterogeneities also significantly influence the maximum exit concentrations at the beach face. For example, for fields 2 and 4 the maximum exit concentrations are reduced by nearly an order of magnitude compared with homogeneous aquifer conditions due to both the enhanced biodegradation of toluene and its increased longitudinal spread.

The variability introduced by aquifer heterogeneity illustrates the difficulties associated with accurately predicting the fate of toluene in the subsurface and its subsequent flux across the aquifer-ocean interface even when an aquifer system is relatively well-characterized. Nevertheless, the simulations reveal that regardless of the specific heterogeneities, the biodegradation of toluene in the subsurface is strongly controlled by both toluene's subsurface residence time and the availability of oxygen in the intertidal salt-freshwater mixing zone. Moreover for all cases considered the removal of toluene in the subsurface is significantly enhanced (> 65%) by tidal effects.

4. Conclusions

Numerical simulations revealed that tidal effects may enhance the attenuation of BTEX compounds in an unconfined near-shore aquifer before their discharge to coastal waters. Tide-induced seawater circulations set up a reactive mixing zone in the

ACCEPTED MANUSCRIPT

intertidal region between the discharging contaminated groundwater and oxygenated recirculating seawater. Significant aerobic biodegradation of BTEX was shown to occur in this mixing zone leading to a reduction in the total mass of BTEX transported from the aquifer to ocean and the rate of chemical discharge. Consequently, tides are expected to lessen the threat of BTEX compounds released in a coastal aquifer on the interstitial beach and receiving estuarine and marine ecosystems. For the conditions simulated, tidal forcing reduced the exit concentrations of the BTEX compounds considered, except for benzene, to levels below those set by standard water quality guidelines. Such positive tidal effects may reduce the need to implement engineering remediation strategies to enhance the removal of contaminants before they discharge to coastal waters.

Simulations further showed that enhanced natural attenuation of toluene (and other BTEX compounds) is likely at sites where the tidal forcing dominates over the inland forcing. This is because the tide counter-balanced by the inland flow controls the magnitude of tide-induced seawater recirculation, the extent of mixing between seawater and discharging groundwater, and the contaminants' specific subsurface discharge pathway and residence time. In addition the extent of biodegradation was shown to be limited by the availability of oxygen in the intertidal mixing zone. This availability depends on the rate of oxygen input (i.e., rate of seawater recirculation) relative to the rate of natural oxygen-consuming processes in the subsurface. While simulations performed with heterogeneous hydraulic conductivity fields illustrated the uncertainty associated with predicting the mass of BTEX discharged, for all simulations tides were shown to enhance attenuation regardless of the complexity of the flow patterns. Moreover, these heterogeneous cases further demonstrated that the extent of biodegradation is strongly controlled by the contaminant's residence time in the inter-

ACCEPTED MANUSCRIPT

tidal aquifer and the availability of oxygen there. In addition to the uncertainties associated with the physical flow and transport processes, it is important to note that the natural geochemical processes and biologically-mediated reactions which affect the extent of biodegradation are significantly more complicated than those represented by the geochemical model we have adopted. Nevertheless, the model predictions provide valuable insight into the importance of the tide-induced salt-freshwater mixing zone on the fate and thus potential impact of terrestrial subsurface BTEX compounds discharging to coastal waters.

ACCEPTED MANUSCRIPT

ACCEPTED MANUSCRIPT

References

[1] Valiela I, Costa J, Foreman K, Teal JM, Howes B, and Aubery D. Transport of groundwater-borne nutrients from watersheds and their effects on coastal waters. *Biogeochemistry* 1990;10:177-97.

[2] LaRoche J, Nuzzi R, Waters R, Wyman K, Falkowski PG, and Wallace D. Brown tide blooms in Long Island's coastal waters linked to interannual variability in groundwater flow. *Global Change Biology* 1997;3:397-410.

[3] Lapointe BE and O'Connell JD. Nutrient-enhanced growth of Cladophora prolifera in Harrington Sound, Bermuda: Eutrophication of a confined, phosphorus-limited marine ecosystem. *Estuarine, Coastal and Shelf Science* 1989;28:347-60.

[4] Valiela I, Foreman K, LaMontagne M, Hersh D, Costa J, Peckol P, DeMeaAndreson B, D'Avanzo C, Babione M, Sham C, Brawley J, and Lajtha K. Coupling of watersheds and coastal waters: Sources and consequences of nutrient enrichment in Waquoit Bay, Massachusetts. *Estuaries* 1992;15(4):443-57.

[5] McLachlan A and Turner I. The interstitial environment of sandy beaches. *Marine Ecology* 1994;15(3-4):177-211.

[6] Slomp CP and van Cappellen P. Nutrient inputs to the coastal ocean through submarine groundwater discharge: controls and potential impact. *Journal of Hydrology* 2004;295:64-86.

[7] Robinson C, Gibbes B, Carey H, and Li L. Salt-freshwater dynamics in a subterranean estuary over a spring-neap tidal cycle. *Journal of Geophysical Research* 2007;112:C09007. doi:10.1029/2006JC003888.

[8] Charette MA and Sholkovitz ER. Trace element cycling in a subterranean estuary: Part 2. Geochemistry of the pore water. *Geochem et Cosmochim Acta* 2006;70:811-26.

ACCEPTED MANUSCRIPT

619 [9] Ullman WJ, Chang B, Miller DC, and Madsen JA. Groundwater mixing, nutrient
620 diagenesis, and discharges across a sandy beachface, Cape Henlopen, Delaware
621 (USA). *Estuarine, Coastal and Shelf Science* 2003;57:539-52.
622 [10] Robinson C, Li L, and Barry DA. Effect of tidal forcing on a subterranean estu-
623 ary. *Advances in Water Resources* 2007;30:851-65.
624 [11] Werner AD and Lockington DA. Tidal impacts on riparian salinities near estuar-
625 ies. *Journal of Hydrology* 2006;328(3-4):511-22.
626 [12] Mao X, Enot P, Barry DA, Li L, Binley A, and Jeng D-S. Tidal influence on be-
627 haviour of a coastal aquifer adjacent to a low-relief estuary. *Journal of Hydrology*
628 2006;327:110-27.
629 [13] Ataie-Ashtiani B, Volker RE, and Lockington DA. Tidal effects on sea water in-
630 trusion in unconfined aquifers. *Journal of Hydrology* 1999;216:17-31.
631 [14] Prieto C and Destouni G. Quantifying hydrological and tidal influences on
632 groundwater discharges to coastal waters. *Water Resources Research*
633 2005;41:W12427. doi:20.1029/2004WR003920.
634 [15] Robinson MA, Gallagher D, and Reay W. Field observations of tidal and sea-
635 sonal variations in groundwater discharge to tidal estuarine surface water. *Ground*
636 *Water Monitoring and Remediation* 1998;18(1):83-92.
637 [16] Robinson C, Gibbes B, and Li L. Driving mechanisms for flow and salt transport
638 in a subterranean estuary. *Geophysical Research Letters* 2006;33:L03402.
639 doi:10.1029/2005GL025247.
640 [17] Vandenbohede A and Lebbe L. Occurrence of salt water above fresh water in dy-
641 namic equilibrium in a coastal groundwater flow system near De Panne, Belgium.
642 *Hydrogeology Journal* 2005;14(4):462 - 72.

ACCEPTED MANUSCRIPT

643 [18] Mango AJ, Schmeeckle MW, and Furbish DJ. Tidally induced groundwater cir-
644 culation in an unconfined coastal aquifer modeled with a Hele-Shaw cell. *Geology*
645 2004;32(3):233-36.
646 [19] Boufadel MC. A mechanistic study of nonlinear solute transport in a groundwa-
647 ter-surface water system under steady state and transient hydraulic conditions. *Water*
648 *Resources Research* 2000;36(9):2549-65.
649 [20] Turner IL and Acworth RI. Field measurements of beachface salinity structure
650 using cross-borehole resistivity imaging. *Journal of Coastal Research*
651 2004;20(3):753-60.
652 [21] Ghyben WB. Notes in verband met voorgenomen put boring Nabji Amsterdam.
653 Tijdschrift van let koninklijk Institut van Ingeniers, 1899.
654 [22] Herzberg A. Die Wasserversorgung einiger Nordseebder. *Zeitshriftfur Gas-*
655 *beleuchtung und Wasserversorgung* 1901;44:815–19.
656 [23] Li L, Barry DA, Stagnitti F, and Parlange J-Y. Submarine groundwater discharge
657 and associated chemical input to a coastal sea. *Water Resources Research*
658 1999;35(11):3253-59.
659 [24] Robinson C, Li L, and Prommer H. Tide-induced recirculation across the aquifer-
660 ocean interface. *Water Resources Research* 2007;43:W07428.
661 doi:10.1029/2006WR005679.
662 [25] Moore WS. The subterranean estuary: A reaction zone of ground water and sea
663 water. *Marine Chemistry* 1999;65:111-25.
664 [26] Spiteri C, Regnier P, Slomp CP, and Charette MA. pH-dependent iron oxide pre-
665 cipitation in a subterranean estuary. *Journal of Geochemical Exploration*
666 2005;88:399-403.

ACCEPTED MANUSCRIPT

667 [27] Li L, Barry DA, Jeng DS, and Prommer H. Tidal dynamics of groundwater flow
668 and contaminant transport in coastal aquifers. In: Cheng AHD and Ouazar D, editors.
669 Coastal aquifer management: monitoring, modelling and case studies. United States:
670 Lewis Publishers; 2004.
671 [28] Boufadel MC, T SM, and Venosa AD. Tracer studies in laboratory beach simu-
672 lating tidal influences. *Journal of Environmental Engineering - ASCE*
673 2006;132(6):616-23.
674 [29] Li HL, Zhao QH, Boufadel MC, and Venosa AD. A universal nutrient applica-
675 tion strategy for the bioremediation of oil-polluted beaches. *Marine Pollution Bulletin*
676 2007;54(8):1146-61.
677 [30] Westbrook SJ, Rayner JL, Davis GB, Clement TP, Bjerg PL, and Fisher SJ. In-
678 teraction between shallow groundwater, saline surface water and contaminant dis-
679 charge at a seasonally and tidally forced estuarine boundary. *Journal of Hydrology*
680 2005;302:255-69.
681 [31] Trefry MG, Svensson TJA, and Davis GB. Hypoaigic influences on groundwater
682 flux to a seasonally saline river. *Journal of Hydrology* 2007;335(3-4):330-53.
683 [32] Mao X, Prommer H, Barry DA, Langevin CD, Panteleit B, and Li L. Three-
684 dimensional model for multi-component reactive transport with variable density
685 groundwater flow. *Environmental Modelling & Software* 2006;21:615-28.
686 [33] Guo W and Langevin CD. User's Guide to SEAWAT: A computer program for
687 simulation of three-dimensional variable-density ground-water flow. US Geological
688 Survey, Techniques of Water-Resources Investigations 6-A7; 2002.
689 [34] Parkhurst DL and Appelo CAJ. User's guide to PHREEQC (version 2) - A com-
690 puter program for speciation, batch-reaction, one dimensional transport, and inverse

ACCEPTED MANUSCRIPT

691 geochemical calculations. US Department of the Interior, Water-Resources Investiga-
692 tions Report 99-4259, 1999.
693 [35] Barry DA, Prommer H, Miller CT, Engesgaard P, Brun A, and Zheng C. Model-
694 ling the fate of oxidisable organic contaminants in groundwater. *Advances in Water*
695 *Resources* 2002;25:945-83.
696 [36] Kristensen E. Organic matter diagenesis at the oxic/anoxic interface in marine
697 sediments, with emphasis on the role of burrowing animals. *Hydrobiologia*
698 2000;426:1-24.
699 [37] House WA. Factors influencing the extent and development of the oxic zone in
700 sediments. *Biogeochemistry* 2003;63:319-33.
701 [38] Charette MA, Sholkovitz ER, and Hansel CM. Trace element cycling in a subter-
702 ranean estuary: Part 1. Geochemistry of the permeable sediments. *Geochem et Cos-*
703 *mochim Acta* 2005;69(8):2095-109.
704 [39] Brown AC and McLachlan A. Ecology of sandy shores. Amsterdam: Elsevier,
705 1990.
706 [40] Ueda S, Go CU, and Suzumura M. Denitrification in a seashore sandy deposit
707 influenced by groundwater discharge. *Biogeochemistry* 2003;63:187-205.
708 [41] Riedl RJ and Machan R. Hydrodynamic patterns in lotic intertidal sands and their
709 bioclimatological implications. *Marine Biology* 1972;13:179-209.
710 [42] World Health Organization. Guidelines for drinking-water quality, Volume 1,
711 Recommendations. 2006.
712 [43] World Health Organization. Guidelines for safe recreational water environments.
713 Volume 1, Coastal and fresh waters. 2003.
714 [44] Hem JD. Study and interpretation of chemical characteristics of natural water.
715 Alexandria, VA: U. S. Geological Survey, 1985.

ACCEPTED MANUSCRIPT

716 [45] Frenzel H. A field generator based on Mejia's algorithm. Institut fr Umwelt-
717 physik, University of Heidelberg, 1995.
718 [46] Gelhar LW. Stochastic subsurface hydrology. New Jersery: Prentice Hall, 1993.
719 [47] Alagappan G and Cowan RM. Effect of temperature and dissolved oxygen on the
720 growth kinetics of Pseudomonas putida F1 growing on benzene and toluene. *Chemos-*
721 *phere* 2004;54:1255-65.
722 [48] Schirmer M, Butler BJ, Roy JW, Frind EO, and Barker JF. A relative-least-
723 squares technique to determine unique Monod kinetic parameters of BTEX com-
724 pounds using batch experiment. *Journal of Contaminant Hydrology* 1999;37:69-86.
725

ACCEPTED MANUSCRIPT

ACCEPTED MANUSCRIPT

726 **Table Captions**

727 Table 1. Concentrations of aqueous components.

728 Table 2. Aerobic degradation reactions and Monod kinetic parameter values for

729 BTEX compounds.

ACCEPTED MANUSCRIPT

ACCEPTED MANUSCRIPT

730 **Figure Captions**

731 Figure 1. Tide-induced (a) salt distribution, (b) oxygen distribution with no natural
732 oxygen-consuming processes (b_O = 0) and (c) oxygen distribution with natural
733 oxygen consumption (b_O = 0.09 d^{-1}) in a tidally-influenced near-shore aquifer
734 (base conditions). The upper saline plume (USP), saltwater wedge and fresh-
735 water discharge zone (FDZ) are denoted in (a). The arrows represent the
736 groundwater flows averaged over a tidal cycle.

737 Figure 2. Model geometry and boundary conditions. The model domain is divided
738 into two zones: a surface water zone (Zone A, not shaded) and an aquifer zone
739 (Zone B, shaded).

740 Figure 3. Concentrations of toluene (a-c), biomass (d-f) and oxygen (g-i) 75 d, 100 d
741 and 125 d after injection of toluene for simulation with aerobic biodegradation
742 and b_O = 0.09 d^{-1} but no tidal forcing. The arrows represent the steady state
743 flow. The contour lines depict the salt distribution in the near-shore aquifer
744 where the contour levels (fraction seawater) are the same for all subplots and
745 are notated in (d). Note that there is only minor biomass growth close to the
746 shoreline (evident 75 d and 100 d after injection) for these conditions.

747 Figure 4. Concentrations of toluene (a-c), biomass (d-f) and oxygen (g-i) 75 d, 100 d
748 and 125 d after injection of toluene for simulation with tidal forcing, aerobic
749 biodegradation and b_O = 0.09 d^{-1}. The arrows represent the tide-averaged
750 groundwater flow. The contour lines depict the salt distribution in the near-
751 shore aquifer where the contour levels (fraction seawater) are the same for all
752 subplots and are notated in (d).

ACCEPTED MANUSCRIPT

Figure 5. (a) Total moles of toluene, (b) change in total moles of biomass and (c) change in total moles of oxygen in the aquifer following toluene injection for simulations without tides and without biodegradation (–·–), without tides but with biodegradation and b_O = 0.09 d^{-1} (···), with tides but without biodegradation (–×–), with tides, biodegradation and b_O = 0 d^{-1} (–) and with tides, biodegradation and b_O = 0.09 d^{-1} (– –).

Figure 6. Total toluene flux across the aquifer-ocean interface versus time since toluene injection for simulation without tides and without biodegradation (–), without tides but with biodegradation (···), with tides but without biodegradation (–×–) and with tides and biodegradation (– –). For all simulations b_O = 0.09 d^{-1}.

Figure 7. Toluene exit concentrations along the aquifer-ocean interface for simulations (a) without tides and without biodegradation, (b) without tides but with biodegradation, (c) with tides but without biodegradation, and (d) with tides and with biodegradation. Results are shown for 75 d (–·–), 100 d (···), 125 d (–) and 150 d (–×–) after toluene injection. Note the changes in vertical scale.

Figure 8. Total flux of benzene (– –), toluene (···), ethylbenzene (–×–) and xylenes (–) across the aquifer-ocean interface versus time since BTEX injection for simulations (a) with and (b) without tides. The exit concentrations along the aquifer-ocean interface for each component (c) 140 d after BTEX injection with tides present and (d) 80 d after BTEX injection in the absence of tides are also shown. The WHO guideline concentrations [42] for benzene (0.13 μmol

ACCEPTED MANUSCRIPT

776 l^{-1}), toluene (7.6 µmol l^{-1}), ethylbenzene (2.8 µmol l^{-1}) and xylenes (4.7 µmol
777 l^{-1}) are indicated in (c) and (d). Note the change in vertical scale between (c)
778 and (d).

779 Figure 9. Influence of tidal amplitude on (a) the removal efficiency of toluene in the
780 subsurface prior to discharge and (b) Q_t (tidally-driven seawater recirculation)
781 across the aquifer-ocean interface.

782 Figure 10. Relationship between Q_f / Q_t (ratio of fresh groundwater discharge to tidal-
783 ly-driven seawater recirculation) and the removal efficiency of toluene in the
784 subsurface prior to discharge. Circles indicate results from simulations with
785 tidal amplitude varied from the base conditions and crosses indicate results
786 from simulations with Q_f varied from the base conditions.

787 Figure 11. Influence of the first-order oxygen decay constant (b_O) on (a) the total
788 moles of oxygen in the aquifer and (b) the removal efficiency of toluene in the
789 subsurface prior to discharge.

790 Figure 12. Total toluene flux across the aquifer-ocean interface versus time since tolu-
791 ene injection (a) without biodegradation and (b) with biodegradation for ho-
792 mogeneous aquifer conditions (–) and heterogeneous conductivity fields 1 (–
793 –), 2 (–×–), 3 (···) and 4 (–·–). Note the change in vertical scale between (a)
794 and (b).

ACCEPTED MANUSCRIPT

795 **Table 1.** Concentrations of aqueous components.

Component	Initial concentration in Zone B and concentration in Q_f (mmol l^{-1})	Constant concentration in Zone A (mmol l^{-1})	Concentration in contaminant source (mmol l^{-1})
Toluene	0	0	5
Benzene	0	0	7
Ethylbenzene	0	0	1.5
Xylenes	0	0	1.5
Oxygen	0.025	0.25	0.025
Biomass	1.8×10^{-3}	1.8×10^{-3}	1.8×10^{-3}
NaCl	0.01	600 (~ 35 g/l)	0.01

796

ACCEPTED MANUSCRIPT

ACCEPTED MANUSCRIPT

797 **Table 2**. Aerobic biodegradation reactions and Monod kinetic parameter values for

798 BTEX compounds.

Parameter	Value	Reference
Toluene		
Reaction	$C_7H_8 + 9\ O_2 = 7\ CO_2 + 4\ H_2O$	
$\mu_{max\_Toluene}$	8.6 d^{-1}	[47]
$K_{s\_Toluene}$	0.0076 mmol l^{-1}	[47]
$Y_{Toluene}$	0.6	[47]
Benzene		
Reaction	$C_6H_6 + 7.5\ O_2 = 6\ CO_2 + 3\ H_2O$	
$\mu_{max\_Benzene}$	8.4 d^{-1}	[47]
$K_{s\_Benzene}$	0.03 mmol l^{-1}	[47]
$Y_{Benzene}$	0.6	[47]
Ethylbenzene		
Reaction	$C_8H_{10} + 10.5\ O_2 = 8\ CO_2 + 5\ H_2O$	
$\mu_{max\_Ethylbenzene}$	8.5 d^{-1}	Estimated from [48]
$K_{s\ Ethylbenzene}$	0.05 mmol l^{-1}	Estimated from [48]
$Y_{Ethylbenzene}$	0.6	[47]
Xylenes		
Reaction	$C_8H_{10} + 10.5\ O_2 = 8\ CO_2 + 5\ H_2O$	
μ_{max_Xylene}	8.5 d^{-1}	Averaged from [48]
K_{s_Xylene}	0.065 mmol l^{-1}	Averaged from [48]
Y_{Xylene}	0.6	[47]
Aerobe Biomass		
K_{s_O}	0.036 mmol l^{-1}	[47]
b_b	0.1 d^{-1}	[35]

799

ACCEPTED MANUSCRIPT

ACCEPTED MANUSCRIPT

Fig.1

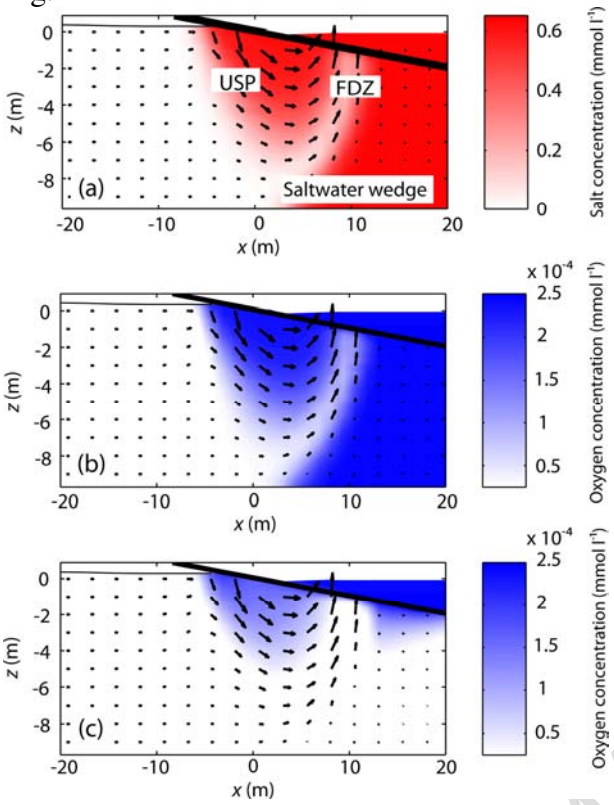

ACCEPTED MANUSCRIPT

ACCEPTED MANUSCRIPT

Fig.2

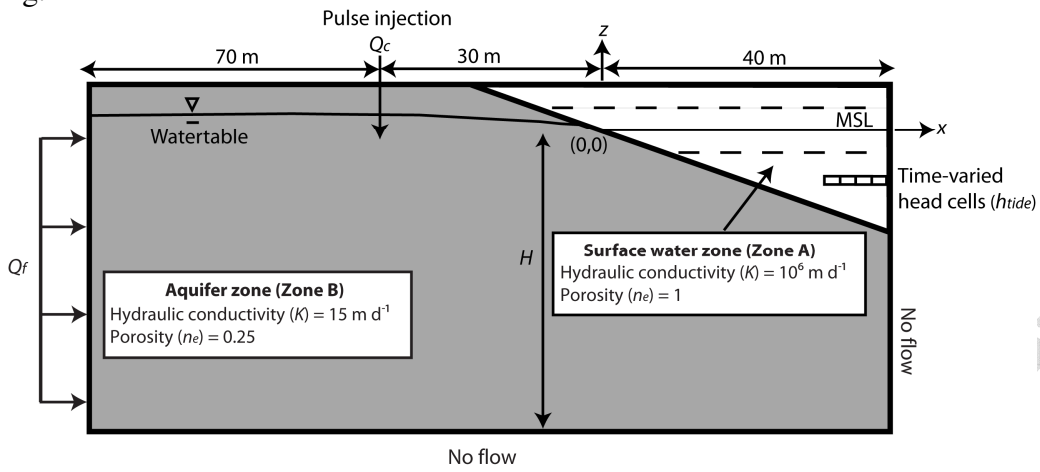

ACCEPTED MANUSCRIPT

ACCEPTED MANUSCRIPT

Fig.3

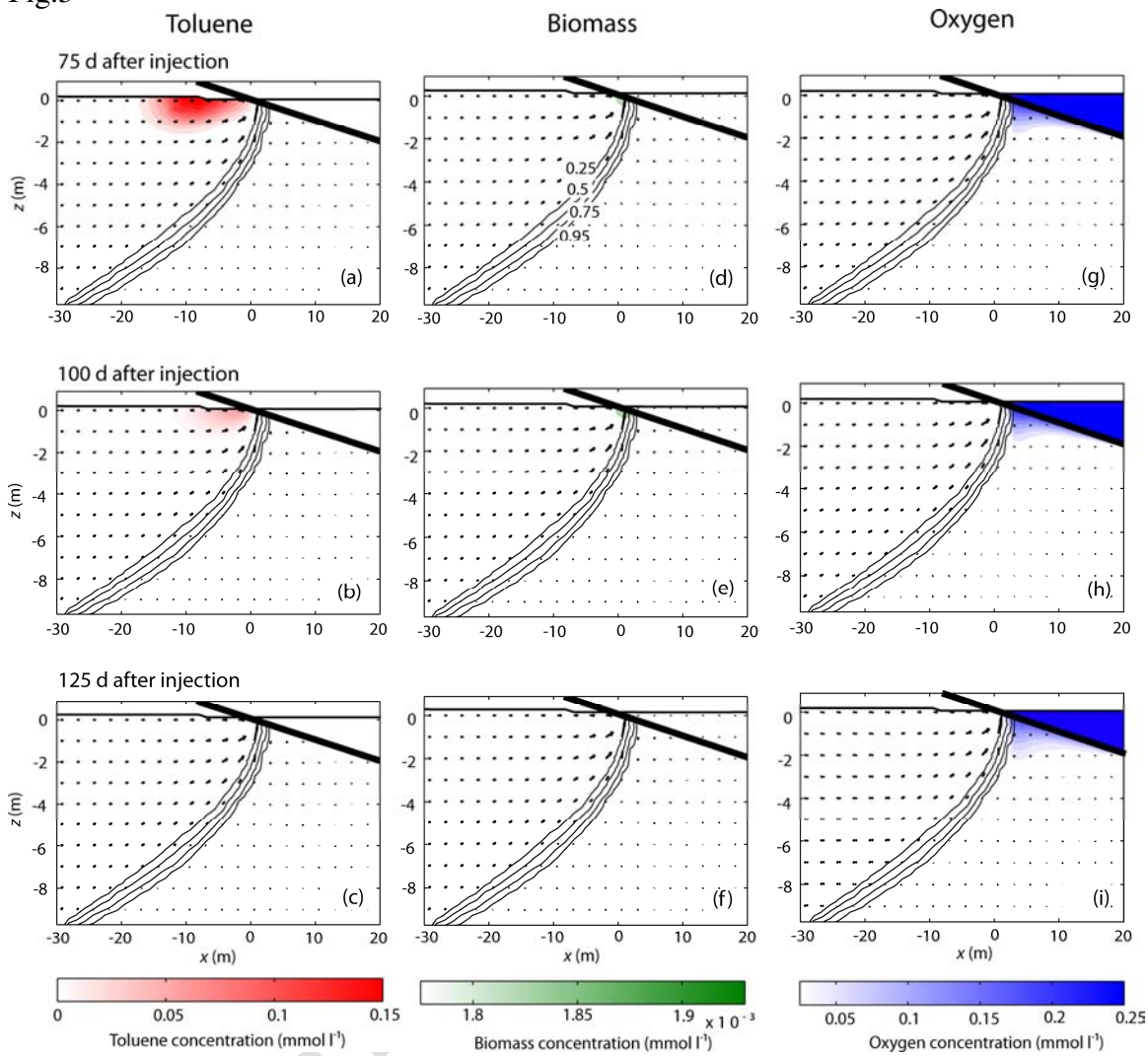

ACCEPTED MANUSCRIPT

Fig.4

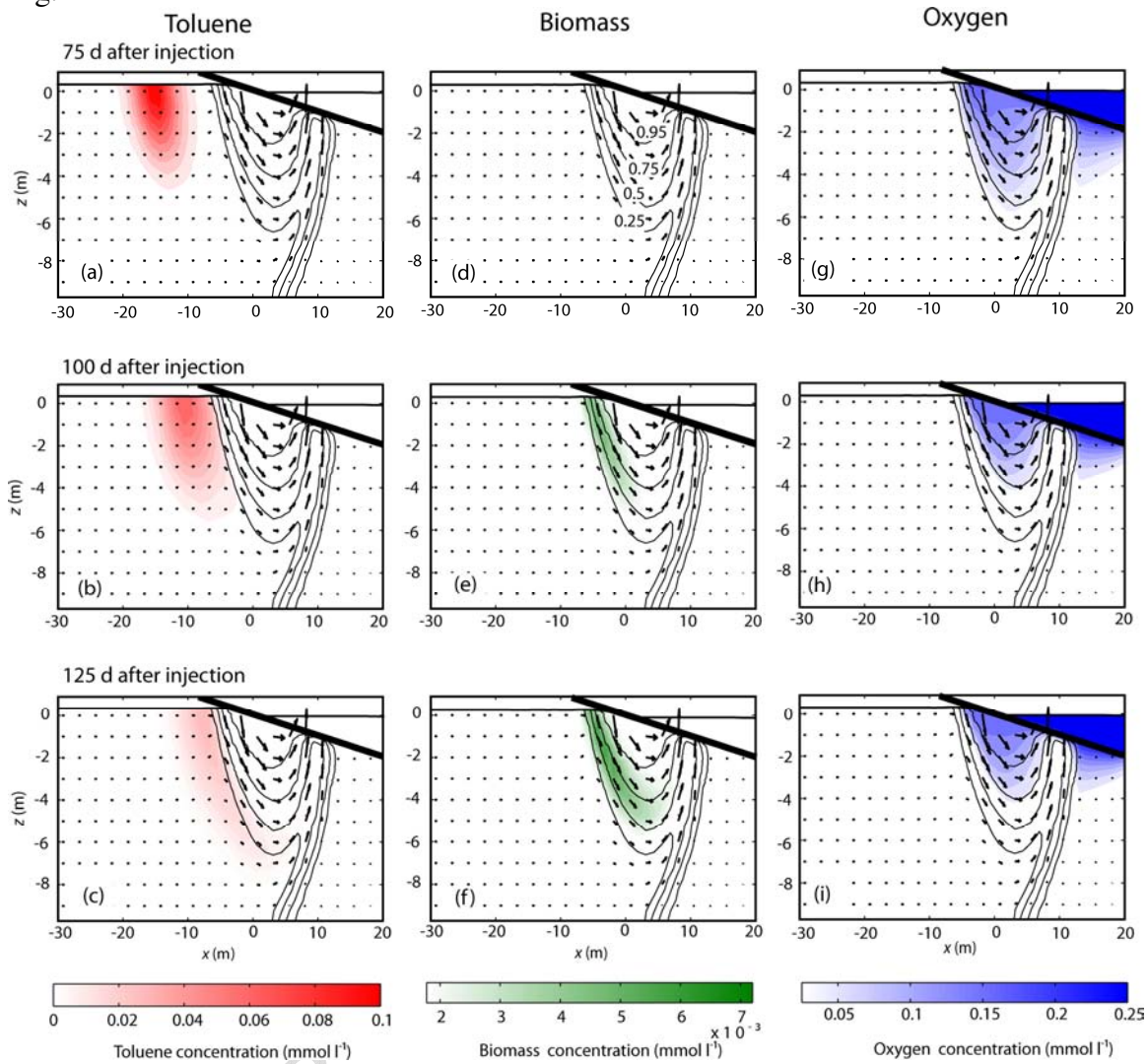

ACCEP

ACCEPTED MANUSCRIPT

Fig.5

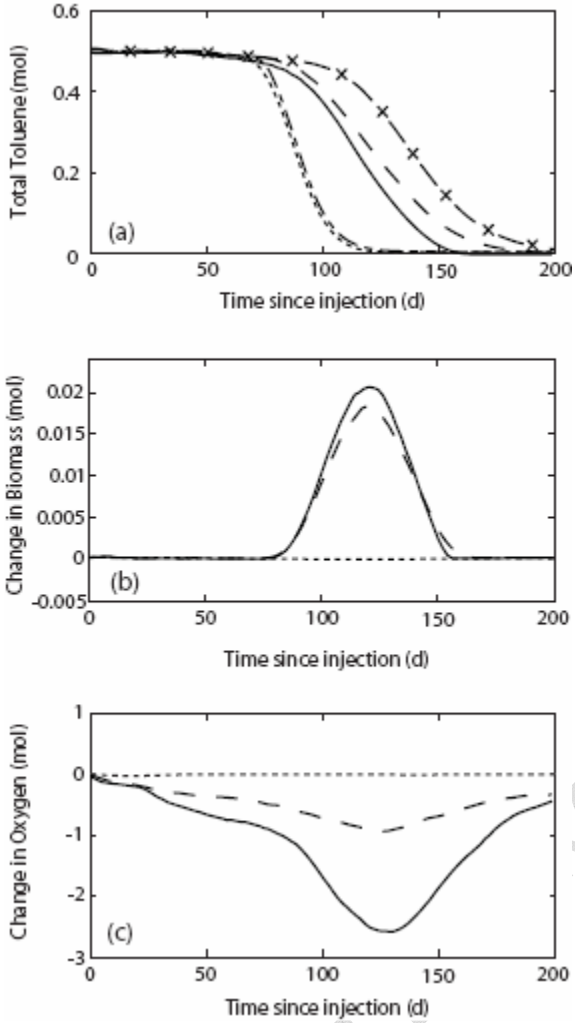

ACCEPTED MANUSCRIPT

ACCEPTED MANUSCRIPT

Fig.6

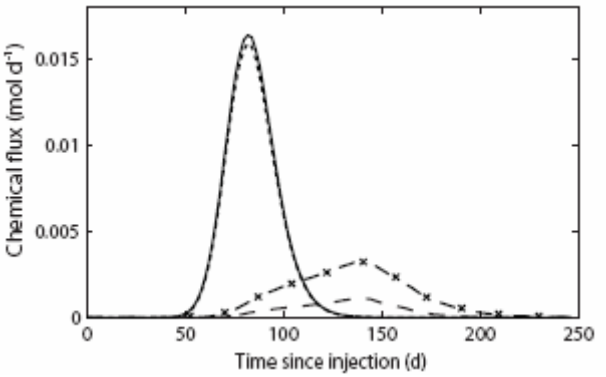

ACCEPTED MANUSCRIPT

ACCEPTED MANUSCRIPT

Fig.7

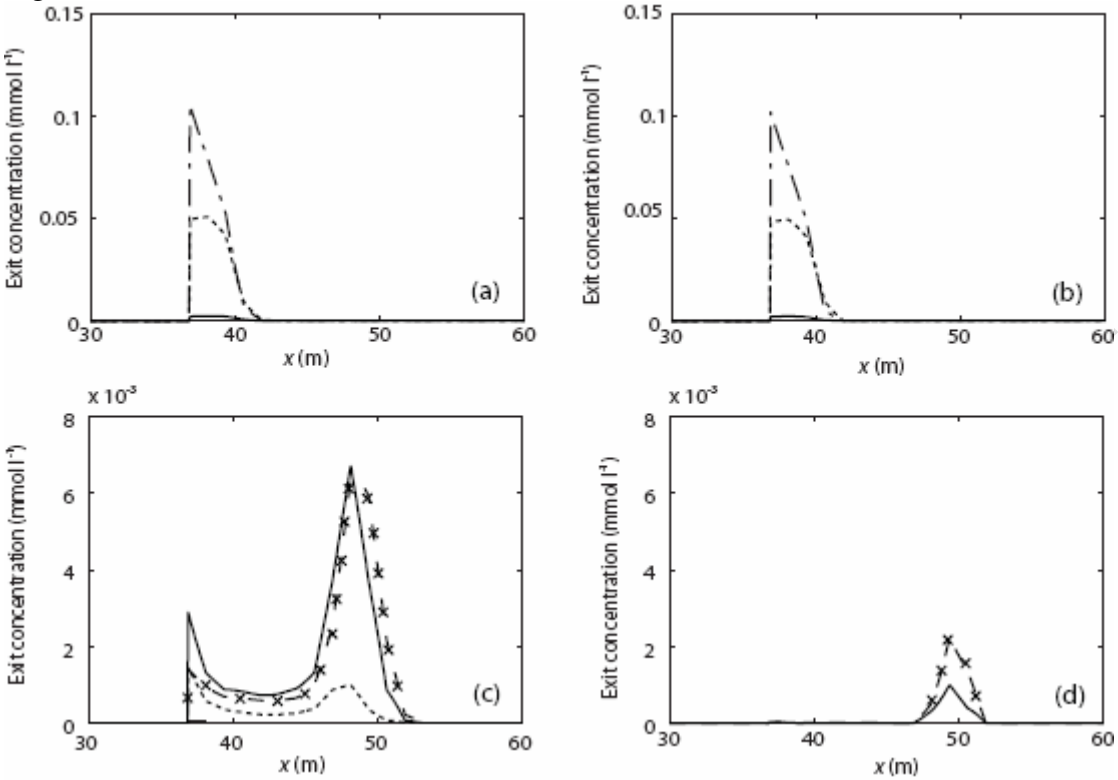

ACCEPTED MANUSCRIPT

Fig.8

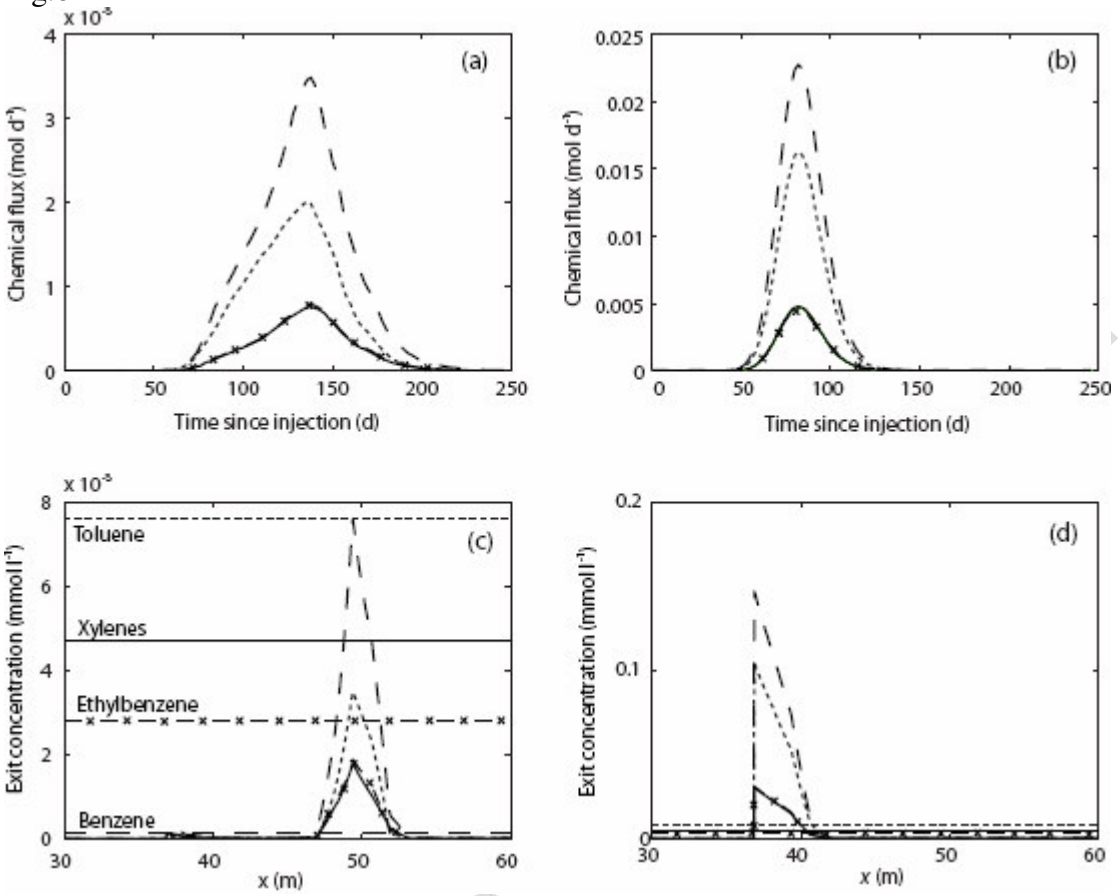

ACCEPTED

ACCEPTED MANUSCRIPT

Fig.9

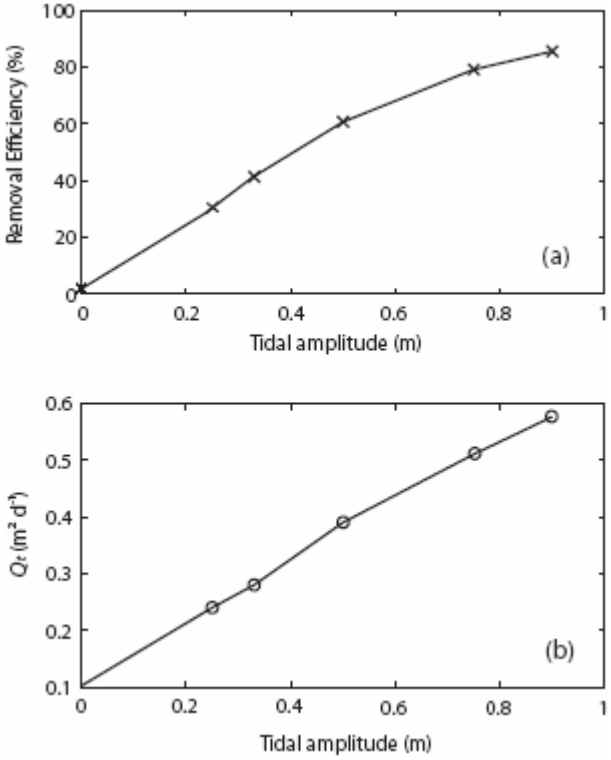

ACCEPTED MANUSCRIPT

ACCEPTED MANUSCRIPT

Fig.10

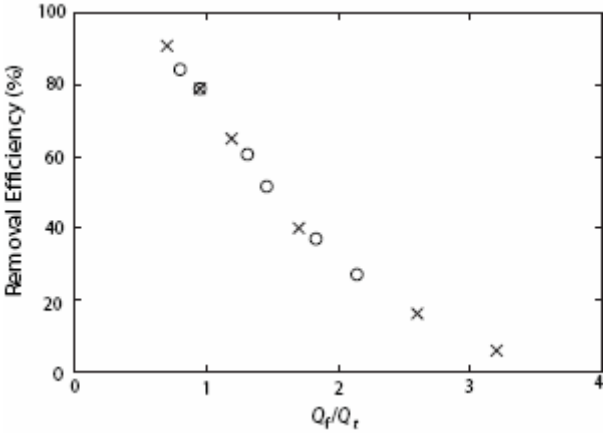

ACCEPTED MANUSCRIPT

ACCEPTED MANUSCRIPT

Fig.11

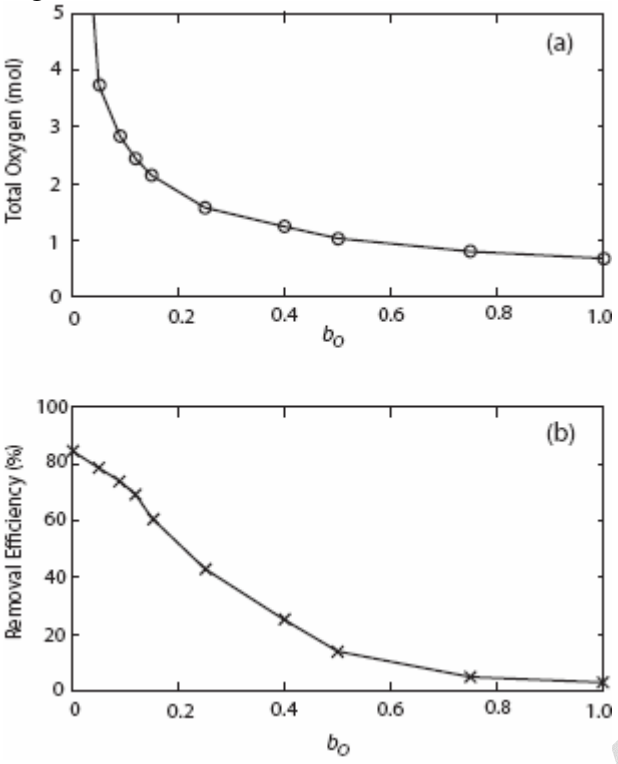

ACCEPTED MANUSCRIPT

ACCEPTED MANUSCRIPT

Fig.12